

ARTICLE TYPE

Properties of the QGP created in heavy-ion collisions

P. Moreau¹ | O. Soloveva² | I. Grishmanovskii² | V. Voronyuk³ | L. Oliva² | T. Song⁴ | V. Kireyeu³ | G. Coci⁴ | E. Bratkovskaya^{*4,2}

¹Department of Physics, Duke University, Durham, NC 27708, USA

²Institute for Theoretical Physics, University of Frankfurt, Frankfurt, Germany

³Joint Institute for Nuclear Research, Joliot-Curie 6, 141980 Dubna, Moscow Region, Russia

⁴GSI, Helmholtzzentrum für Schwerionenforschung GmbH, Darmstadt, Germany

Correspondence

* GSI, Darmstadt, Germany Email: E.Bratkovskaya@gsi.de

We review the properties of the strongly interacting quark-gluon plasma (QGP) at finite temperature T and baryon chemical potential μ_B as created in heavy-ion collisions at ultrarelativistic energies. The description of the strongly interacting (non-perturbative) QGP in equilibrium is based on the effective propagators and couplings from the Dynamical QuasiParticle Model (DQPM) that is matched to reproduce the equation-of-state of the partonic system above the deconfinement temperature T_C from lattice QCD. Based on a microscopic transport description of heavy-ion collisions we discuss which observables are sensitive to the QGP creation and its properties.

KEYWORDS:

heavy-ions, quark-gluon plasma, transport models quark-gluon plasma

1 | INTRODUCTION

An understanding of the structure of our universe is an intriguing topic of research in our Millennium, which combines the efforts of physicists working in different fields of astrophysics, cosmology and heavy-ion physics (Strassmeier et al., 2019). The common theoretical efforts and modern achievements in experimental physics allowed to make a substantial progress in understanding the properties of the nuclear matter and extended our knowledge of the QCD phase diagram which contains the information about the properties of our universe from the early beginning – directly after the Big Bang – when the matter was in a quark-gluon plasma (QGP) phase at very high temperature T and practically zero baryon chemical potential μ_B , to the later stages of the universe, where in the expansion phase stars and galaxies have been formed. In the later phase, the matter is at low temperature, however, at very large baryon densities or baryon chemical potential μ_B . The range of the phase diagram at large μ_B and low temperature T can also be explored in the astrophysical context (Klahn et al., 2006), such as in the dynamics of supernovae or in the dynamics of neutron-star mergers and gravitational waves. Collisions of heavy-ions at ultra-relativistic energies –

e.g. at the Relativistic Heavy Ion Collider (RHIC) or the Large Hadron Collider (LHC) – provide the possibility to reproduce on Earth the conditions closer to the Big Bang, when the matter was in a QGP phase of unbound quarks and gluons at very high temperature and almost vanishing μ_B . Indeed, in experiments it is possible to achieve a QGP only in extremely small volumes, moreover, the fast expansion leads to a fast hadronization of the QGP such that only final hadrons and leptons are measured. Thus, it is quite challenging to investigate the properties of the QGP experimentally.

The region of phase diagram at finite T and μ_B is of special interest nowadays. According to lattice calculations of quantum chromodynamics (lQCD) (Aoki et al., 2009; Aoki, Endrodi, Fodor, Katz, & Szabo, 2006; Bazavov et al., 2012; Bernard et al., 2005; J. Guenther et al., 2017), the phase transition from hadronic to partonic degrees of freedom at small baryon chemical potential $\mu_B \leq 350$ MeV is a crossover. According to phenomenological models (e.g. recent PNJL calculations (Fuseau, Steinert, & Aichelin, 2020)), the crossover is expected to turn into a first order transition at some critical point (T_{cr}, μ_{cr}) in the phase diagram with increasing baryon chemical potential μ_B . However, the theoretical predictions concerning the location of the critical point are rather uncertain. From the experimental side the beam energy scan (BES)

program at RHIC aims to find the critical point and the phase boundary by scanning the collision energy (Kumar, 2011; Mohanty, 2011). Moreover, new facilities such as FAIR (Facility for Antiproton and Ion Research) and NICA (Nuclotron-based Ion Collider fAcility) are presently under construction; they will explore the intermediate energy regime of rather large baryon densities and moderate temperatures where one might also study the competition between chiral symmetry restoration and deconfinement as advocated in Refs. (Cassing, Palmese, Moreau, & Bratkovskaya, 2016; Palmese et al., 2016).

From the theoretical side it is quite challenging to investigate the "intermediate" region of the QCD phase diagram of non-vanishing quark (or baryon) densities from first principles due to the so called "sign problem" which prevents the IQCD calculations to be extended to large μ_B (cf. (J. N. Guenther, 2020)). Our present knowledge on QCD in Minkowski space for non-vanishing μ_B are based mainly on effective approaches. Using effective models, one can study the properties of QCD in equilibrium, i.e., thermodynamic quantities, the Equation-of-State (EoS) of the QGP as well as transport coefficients. The dynamical quasiparticle model (DQPM) has been introduced for that aim (Berrehrah, Bratkovskaya, Steinert, & Cassing, 2016; Cassing, 2007a, 2007b; Linnyk, Bratkovskaya, & Cassing, 2016; Peshier & Cassing, 2005). It is based on partonic propagators with sizeable imaginary parts of the self-energies incorporated. Whereas the real part of the self-energies can be attributed to a dynamically generated mass (squared), the imaginary parts contain the information about the interaction rates of the degrees-of-freedom. Moreover, the imaginary parts of the propagators define the spectral functions of the 'particles' which might show narrow (or broad) quasiparticle peaks. An important advantage of a propagator based approach is that one can formulate a consistent thermodynamics (Vanderheyden & Baym, 1998) and a causal theory for non-equilibrium states on the basis of Kadanoff–Baym equations (Kadanoff & Baym, 1962).

Since the QGP is formed for a short time in a finite volume in heavy-ion collisions (HICs), it is very important to understand the time evolution of the expanding system. Thus, it is mandatory to have a proper non-equilibrium description of the entire dynamics through different phases - starting with impinging nuclei in their groundstates, going through the QGP phase (showing some approach to equilibration) and end up with the final asymptotic hadronic states. To this aim, the Parton–Hadron–String Dynamics (PHSD) transport approach (Bratkovskaya, Cassing, Konchakovski, & Linnyk, 2011; Cassing, 2009; Cassing & Bratkovskaya, 2008, 2009; Linnyk et al., 2016) has been formulated more than a decade ago (on the basis of the Hadron-String-Dynamics (HSD) approach (Cassing & Bratkovskaya, 1999)), and it was found to

well describe observables from p+A and A+A collisions from SIS (Schwerionensynchrotron) to LHC energies for the bulk dynamics, electromagnetic probes such as photons and dileptons as well as open charm hadrons (Bratkovskaya, Kostyuk, Cassing, & Stoecker, 2004; Linnyk et al., 2016; Linnyk, Konchakovski, Cassing, & Bratkovskaya, 2013; T. Song, Cassing, Moreau, & Bratkovskaya, 2018).

In order to explore the partonic systems at finite μ_B , the PHSD approach has been extended to incorporate partonic quasiparticles and their differential cross sections that depend not only on temperature T as obtained in Ref. (Ozvenchuk, Linnyk, Gorenstein, Bratkovskaya, & Cassing, 2013) and employed in the previous PHSD studies, but also on chemical potential μ_B and center-of-mass energy of colliding partons \sqrt{s} and their angular distributions explicitly (Moreau, 2019; Moreau et al., 2019). Within this extended approach we have studied the 'bulk' observables such as rapidity distributions and transverse momentum spectra in heavy-ion collisions from AGS (Alternating Gradient Synchrotron) to RHIC energies for symmetric and asymmetric (light + heavy nuclear) systems. However, we have found only a small influence of μ_B dependences of parton properties (masses and widths) and partonic interaction cross sections in the bulk observables (Moreau et al., 2019).

Recently we studied the collective flow (v_1, v_2) coefficients for different identified hadrons and their sensitivity to the μ_B dependences of partonic cross sections (Soloveva, Moreau, Oliva, Song, et al., 2020; Soloveva, Moreau, Oliva, Voronyuk, et al., 2020). We have found that the flow coefficients show a small, but visible sensitivity to the μ_B dependence of partonic interactions.

In this work we study the properties of the QGP created in heavy-ion collisions and show the time evolution of the (T, μ_B) distribution, as probed in HICs, and relate it to observables such as multiplicities and collective flow (v_1, v_2) coefficients.

2 | A MICROSCOPIC TRANSPORT DESCRIPTION OF THE NONPERTURBATIVE QGP

In this Section we recall the basic ideas of the PHSD transport approach and the dynamical quasiparticle model (DQPM). The Parton–Hadron–String Dynamics (PHSD) transport approach (Bratkovskaya et al., 2011; Cassing, 2009; Cassing & Bratkovskaya, 2008, 2009; Linnyk et al., 2016) is a microscopic off-shell transport approach for the description of strongly interacting hadronic and partonic matter in and out-of equilibrium. It is based on the solution of Kadanoff–Baym equations in first-order gradient expansion in phase space (Cassing, 2009) which allows to describe in a causal

way the time evolution of nonperturbative interacting systems. Consequently they are applicable for the dynamics of the QGP which approximately behaves as a strongly interacting liquid at finite T due to the growing of the QCD coupling constant in the vicinity of the critical temperature T_C , where pQCD methods are not applicable.

The partonic phase in the PHSD is modelled based on the dynamical quasiparticle model (DQPM) (Cassing, 2007a, 2007b; Peshier & Cassing, 2005). The DQPM has been introduced in Refs. (Cassing, 2007a, 2007b; Peshier & Cassing, 2005) for the effective description of the QGP in terms of strongly interacting quasiparticles - quarks and gluons, where the properties and interactions are adjusted to reproduce lQCD results for the QGP in equilibrium at finite temperature T and baryon chemical potential μ_B (Aoki et al., 2009, 2006; Bazavov et al., 2012; Bernard et al., 2005; J. Guenther et al., 2017). In the DQPM, the quasiparticles are characterized by single-particle Green's functions (in propagator representation) with complex self-energies. The real part of the self-energies is related to the dynamically generated parton masses (squared), whereas the imaginary part provides information about the lifetime and/or reaction rates of the degrees-of-freedom. Thus, in the DQPM the properties of the partons (quarks and gluons) are characterized by broad spectral functions ρ_j ($j = q, \bar{q}, g$), i.e. the partons are off-shell. This differentiates the PHSD from conventional cascade or transport models dealing with on-shell particles, i.e., δ -functions in the invariant mass squared. The quasiparticle spectral functions are assumed to have a Lorentzian form (Linnyk et al., 2016), which are specified by the parton masses and width parameters:

$$\rho_j(\omega, \mathbf{p}) = \frac{\gamma_j}{E_j} \left(\frac{1}{(\omega - E_j)^2 + \gamma_j^2} - \frac{1}{(\omega + E_j)^2 + \gamma_j^2} \right) \quad (1)$$

separately for quarks/antiquarks and gluons ($j = q, \bar{q}, g$). With the convention $E^2(\mathbf{p}^2) = \mathbf{p}^2 + M_j^2 - \gamma_j^2$, the parameters M_j^2 and γ_j are directly related to the real and imaginary parts of the retarded self-energy, e.g., $\Pi_j = M_j^2 - 2i\gamma_j\omega$. The functional forms, i.e. the (T, μ_B) -dependences of the dynamical parton masses and widths are chosen in the spirit of hard-thermal loop (HTL) calculations by introducing three parameters. They are determined by comparison to the calculated entropy density s , pressure P and energy density ϵ from the DQPM to those from lQCD at $\mu_B = 0$ from Ref. (Borsanyi et al., 2012, 2014).

The DQPM also allows to define a scalar mean-field $U_s(\rho_s)$ for quarks and antiquarks which can be expressed by the derivative of the potential energy density with respect to the scalar density $\rho_s(T, \mu_B)$,

$$U_s(\rho_s) = \frac{dV_p(\rho_s)}{d\rho_s}, \quad (2)$$

which is evaluated numerically within the DQPM. Here, the potential energy density is evaluated by:

$$V_p(T, \mu_B) = T_{g-}^{00}(T, \mu_B) + T_{q-}^{00}(T, \mu_B) + T_{\bar{q}-}^{00}(T, \mu_B), \quad (3)$$

where the different contributions T_{j-}^{00} correspond to the space-like part of the energy-momentum tensor component T_j^{00} of parton $j = g, q, \bar{q}$ (cf. Section 3 in Ref. (Cassing, 2007a)). The scalar mean-field $U_s(\rho_s)$ for quarks and antiquarks is repulsive as a function of the parton scalar density ρ_s and shows that the scalar mean-field potential is in the order of a few GeV for $\rho_s > 10 \text{ fm}^{-3}$. The mean-field potential (2) determines the force on a partonic quasiparticle j , i.e., $\sim M_j/E_j \nabla U_s(x) = M_j/E_j dU_s/d\rho_s \nabla \rho_s(x)$, where the scalar density $\rho_s(x)$ is determined numerically on a space-time grid in PHSD.

The quasiparticles - quarks and gluons - which are moving in the self-generated scalar mean-field potential (2) can interact via elastic and inelastic scattering. A two-body interaction strength can be extracted from the DQPM as well from the quasiparticle widths in line with Ref. (Peshier & Cassing, 2005). In the latest version of PHSD (v. 5.0) the following elastic and inelastic interactions are included $qq \leftrightarrow qq$, $\bar{q}\bar{q} \leftrightarrow \bar{q}\bar{q}$, $gg \leftrightarrow gg$, $gg \leftrightarrow g$, $q\bar{q} \leftrightarrow g$, $qg \leftrightarrow qg$, $g\bar{q} \leftrightarrow g\bar{q}$. The backward reactions are defined using 'detailed-balance' with cross sections calculated from the leading order Feynman diagrams employing the effective propagators and couplings $g^2(T/T_c, \mu_B)$ from the DQPM (Moreau et al., 2019). In Ref. (Moreau et al., 2019), the differential and total off-shell cross sections have been evaluated as a function of the invariant energy of the colliding off-shell partons \sqrt{s} for each T, μ_B . We recall that in the early PHSD studies (using version 4.0 and below) the cross sections depend only on T (cf. the detailed evaluation in Ref. (Ozvenchuk et al., 2013)).

In the PHSD5.0 the quasiparticle properties (masses and widths) as well as their interactions, defined by the differential cross sections and mean-field potential, depend on the 'Lagrange parameters' T and μ_B in each computational cell in space-time. The evaluation of T and μ_B , as calculated in the PHSD from the local energy density ϵ and baryon density n_B , is realized by employing the lattice equation of state and by a diagonalization of the energy-momentum tensor from PHSD as described in Ref. (Moreau et al., 2019).

The hadronization, i.e. the transition from partonic to hadronic degrees-of-freedom (and vice versa) is described by covariant transition rates for the fusion of quark-antiquark pairs or three quarks (antiquarks), respectively. The full microscopic description allows to obey flavor current-conservation, color neutrality as well as energy-momentum conservation (Cassing & Bratkovskaya, 2009). Since the dynamical quarks and antiquarks become very massive close to the phase transition, the formed resonant 'prehadronic' color-dipole states ($q\bar{q}$ or qqq) are of high invariant mass, too, and

sequentially decay to the groundstate meson and baryon octets, thus increasing the total entropy during hadronization.

On the hadronic side, PHSD includes explicitly the baryon octet and decouplet, the 0^- - and 1^- -meson nonets as well as selected higher resonances as in the Hadron-String-Dynamics (HSD) approach (Cassing & Bratkovskaya, 1999). Note that PHSD and HSD (without explicit partonic degrees-of-freedom) merge at low energy density, in particular below the local critical energy density $\epsilon_c \approx 0.5 \text{ GeV/fm}^3$ as extracted from the IQCD results in Ref. (Borsanyi et al., 2012, 2014).

3 | THE TRANSPORT PROPERTIES OF THE QGP CLOSE TO EQUILIBRIUM

The transport properties of the QGP close to equilibrium are characterized by various transport coefficients. The transport coefficients play an important role for the hydrodynamic models since they define the properties of the propagating fluid. The shear viscosity η and bulk viscosity ζ describe the fluid's dissipative corrections at leading order. In the hydrodynamic equations, the viscosities appear as dimensionless ratios, η/s and ζ/s , where s is the fluid entropy density. Such specific viscosities are more meaningful than the unscaled η and ζ values because they describe the magnitude of stresses inside the medium relative to its natural scale. Both coefficients η and ζ are generally expected to depend on the temperature T and baryon chemical potential μ_B . While for the hydrodynamic models the transport coefficient are an 'input' and have to be adopted from some models, a fully microscopic description of the QGP dynamics by transport approaches allows to define them from the interactions of the underlying degrees of freedom.

One way to evaluate the viscosity coefficients of partonic matter is the Kubo formalism (Aarts & Martinez Resco, 2002; Fernandez-Fraile & Gomez Nicola, 2006; Kubo, 1957; Lang, Kaiser, & Weise, 2015), which was used to calculate the viscosities for a previous version of the DQPM within the PHSD transport approach in a box with periodic boundary conditions in Ref. (Ozvenchuk et al., 2013) as well as in the more recent study with the DQPM model in Refs. (Moreau et al., 2019; Soloveva, Moreau, & Bratkovskaya, 2020). Another way to calculate transport coefficients is to use the relaxation-time approximation (RTA) as incorporated in Refs. (Albright & Kapusta, 2016; Chakraborty & Kapusta, 2011; Gavin, 1985; Hosoya & Kajantie, 1985). This strategy has been used in our recent studies where we have investigated the transport properties of the QGP in the (T, μ_B) plane based on the DQPM (Moreau et al., 2019; Soloveva, Moreau, & Bratkovskaya, 2020; Soloveva et al., 2019).

We find that the ratios of transport coefficients η/s and ζ/s evaluated within DQPM are in a good agreement with the available IQCD results for pure SU(3) gauge theory (Astrakhantsev, Braguta, & Kotov, 2017, 2018). The η/s ratio shows a minimum at T_c and slightly rises with T , while ζ/s grows at T_c in line with the IQCD data. This shows that the QGP in the PHSD behaves as a strongly interacting nonperturbative system rather than a dilute gas of weakly interacting partons.

4 | PROPERTIES OF QGP IN HEAVY-ION COLLISIONS

In this Section we discuss the properties of the QGP created in heavy-ion collisions in terms of achievable energy densities and temperatures as well as baryon chemical potentials. We start with an illustration in Fig. 1 of a time evolution of central Au+Au collisions (upper row, section view) at a collisional energy of $\sqrt{s_{NN}} = 19.6 \text{ GeV}$ within the PHSD (Moreau, 2019). The snapshots are taken at times $t = 0.005, 1, 2, 4$ and 8 fm/c . The baryons, antibaryons, mesons, quarks and gluons are shown as colored dots.

We show the local temperature T (middle row) and baryon chemical potential μ_B (lower row), as extracted from the PHSD in the region with $y \approx 0$. The black lines (middle row) indicate the critical temperature $T_c = 0.158 \text{ GeV}$.

As follows from the upper part of Fig. 1, the QGP is created in the early phase of collisions and when the system expands, hadronization occurs. One can see that during the overlap phase the T and μ_B are very large (we give a warning that an extraction of the thermodynamic quantities for the strongly non-equilibrium initial stage is not a consistent procedure) and they decrease with time. However even at 8 fm/c there are "hot spots" of QGP at front surfaces of high rapidity.

We investigate now the time evolution of the T and μ_B distribution in for cells having a temperature $T > T_c(\mu_B)$ at midrapidity ($|y_{\text{cell}}| < 1$) for 5% central Pb+Pb collisions at 158 A GeV . Fig. 2 shows this distribution for times $t < 2 \text{ fm/c}$, $2 \text{ fm/c} < t < 4 \text{ fm/c}$ and $t > 4 \text{ fm/c}$. For early times $t < 2 \text{ fm/c}$ the distribution peaks at a temperature of about 0.25 GeV and a sizable chemical potential of about 0.6 GeV while for times in the interval $2 \text{ fm/c} < t < 4 \text{ fm/c}$ the maximum has dropped already to an average temperature $\sim 0.18 \text{ GeV}$ and a chemical potential of about 0.3 GeV . For later times $t > 4 \text{ fm/c}$ the distribution (above T_c) essentially stays around $\mu_B \approx 0.25 \text{ GeV}$. We mention that the values of μ_B probed around the transition temperature T_c in the PHSD are in accordance with the expectation from statistical models, which for central Pb+Pb collisions at 158 A GeV quote a value of $\mu_B = 0.2489 \text{ GeV}$ (Cleymans, Oeschler, Redlich, & Wheaton, 2006).

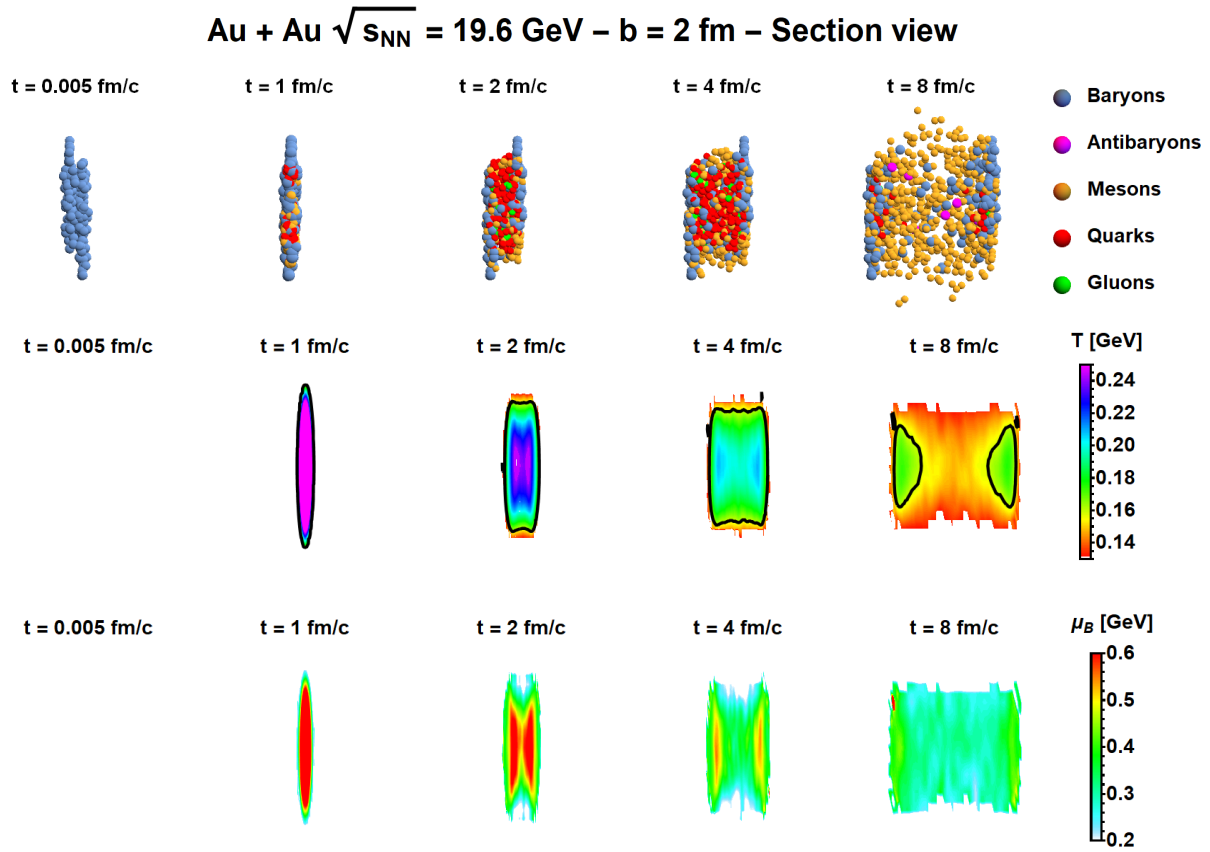


FIGURE 1 Illustration of the time evolution of central Au+Au collisions (upper row, section view) at a collisional energy of $\sqrt{s_{NN}} = 19.6$ GeV within the PHSD (Moreau, 2019). The local temperature T (middle row), baryon chemical potential μ_B (lower row), as extracted from the PHSD for $y \approx 0$. The black lines (middle row) indicate the critical temperature $T_c = 0.158$ GeV.

By varying the collisional energy of the initial nuclei, one can increase or decrease the volume of the QGP produced in the heavy-ion collisions. In Fig. 3 we show the QGP energy fraction versus the total energy for Au+Au at different collisional energies $\sqrt{s_{NN}}$ accounting only the midrapidity region $|y| < 0.5$. One can see that for high energies the QGP fraction is large compared to lower collisional energies where the volume of QGP is small. While at high energy heavy-ion collisions the QGP phase appears suddenly after the initial primary NN collision, at low energies its appearance is smoother since the passing time of the nuclei is longer. Correspondingly, at low energies the QGP lifetime is large, however, the QGP volume is very small; thus its influence on the dynamics is much reduced compared to high energy collisions where practically 90% of matter at midrapidity is in the QGP phase (at least for a short time).

In Fig. 4 we show the average baryon chemical potential (from PHSD simulations) taken around the chemical freeze-out temperature (given by the statistical analysis from Refs. (Adamczyk et al., 2017; Andronic et al., 2010; Cleymans et

al., 2006)). We look only at cells in the midrapidity region to compare with the results from the statistical models. One should stress that we compare two different quantities here: one is μ_B obtained from a statistical analysis of the final particle spectra, and the other is the average μ_B probed in a PHSD simulation around the chemical freeze-out temperature (the latter itself being obtained by a statistical analysis). As one can see in Fig. 4, these two quantities are in a fairly good agreement especially at high energies where μ_B is rather small. At low collisional energies the extracted value of μ_B from the transport calculation (from cells at midrapidity) becomes slightly larger; this might partly be related to the fact that our T, μ_B extraction procedure, optimized for the QGP is not sufficiently accurate for such large values of μ_B/T as probed in this regime. The work on improving the T, μ_B extraction for hadronic dominated matter is in progress.

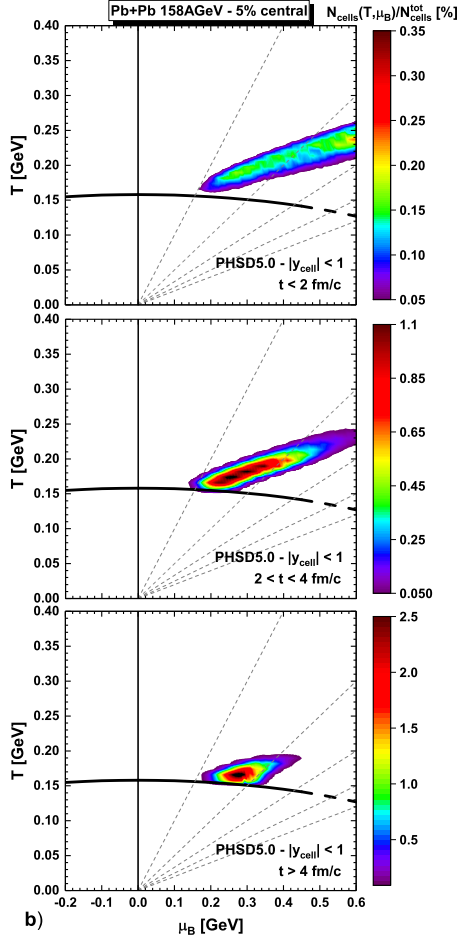


FIGURE 2 Distributions in T and μ_B as extracted from the DQPM equation of state in a PHSD simulation of a central Pb+Pb collision at 158 A GeV for cells with a temperature $T > T_c(\mu_B)$ at midrapidity ($|y_{\text{cell}}| < 1$). The scale corresponds to the number of cells in the PHSD event in the considered bin in $T - \mu_B$ divided by the total number of cells in the corresponding time window (see legend). The solid black line is the DQPM phase boundary for orientation; the gray dashed lines indicate ratios of μ_B/T ranging from 1 to 5 while the vertical line corresponds to $\mu_B = 0$.

5 | OBSERVABLES IN HEAVY-ION COLLISIONS

In our recent study (Moreau et al., 2019) we have investigated the sensitivity of ‘bulk’ observables, such as rapidity and transverse momentum distributions of different hadrons produced in symmetric and asymmetric heavy-ion collisions from AGS to top RHIC energies, on the details of the QGP interactions and the properties of the partonic degrees-of-freedom. For that, we have considered the following three cases: (1) ‘PHSD4.0’: the quasiparticle properties (masses and widths of quarks and gluons) and partonic interaction cross sections

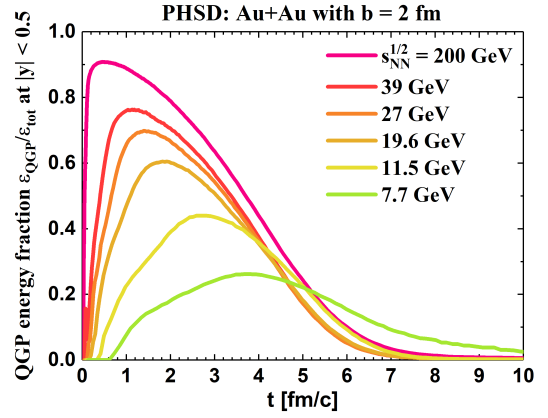


FIGURE 3 The QGP energy fraction from PHSD as a function of time t in central (impact parameter $b = 2$ fm) Au+Au collisions for different collisional energies $\sqrt{s_{NN}}$, taking into account only the midrapidity region $|y| < 0.5$ (Moreau, 2019).

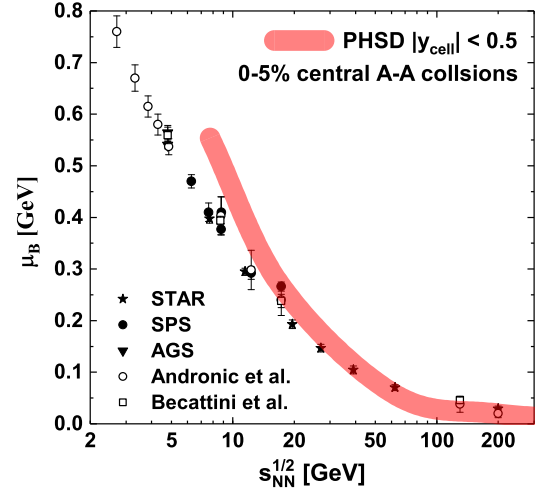


FIGURE 4 Average baryon chemical potential μ_B extracted from PHSD simulations (Moreau, 2019) around the chemical freeze-out temperature T_{ch} in comparison with the values obtained from statistical models (Adamczyk et al., 2017; Andronic et al., 2010; Cleymans et al., 2006).

depend only on T as calculated in Ref. (Ozvenchuk et al., 2013). (2) ‘PHSD5.0 - μ_B ’: the masses and widths of quarks and gluons depend on T and μ_B explicitly; the differential and total partonic cross sections are obtained by calculations of the leading order Feynman diagrams from the DQPM and explicitly depend on invariant energy \sqrt{s} , temperature T and baryon chemical potential μ_B (Moreau et al., 2019). (3) ‘PHSD5.0 - $\mu_B = 0$ ’: the same at (2), but for $\mu_B = 0$.

The comparison of the ‘bulk’ observables for A+A collisions within the three cases of PHSD in Ref. (Moreau et al., 2019) has illuminated that they show a very low sensitivity to

the μ_B dependences of parton properties (masses and widths) and their interaction cross sections such that the results from PHSD5.0 with and without μ_B were very close to each other. Only in the case of kaons, antiprotons \bar{p} and antihyperons $\bar{\Lambda} + \bar{\Sigma}^0$, a small difference between PHSD4.0 and PHSD5.0 could be seen at top SPS and top RHIC energies. This can be understood as follows: as has been illustrated in Section 4, at high energies such as top RHIC where the QGP volume is very large in central collisions, the μ_B is very small, while, when decreasing the collision energy (and consequently increase μ_B) the fraction of the QGP is decreasing such that the final observables are dominated by the hadronic phase. Thus, the probability for the hadrons created at the QGP hadronization to rescatter, decay, or be absorbed in hadronic matter increases strongly; as a result the sensitivity to the properties of the QGP is washed out to a large extend.

In Fig. 5 we present the excitation function of hadron multiplicities at midrapidity $dN/dy|_{y=0}$ as a function of the collisional energy $\sqrt{s_{NN}}$. The symbols correspond to the experimental data, while the lines correspond to the PHSD5.0 calculations including (T, μ_B) for mesons - π^\pm , K^\pm and (anti-)baryons - p , \bar{p} , $\Lambda + \Sigma^0$, $\bar{\Lambda} + \bar{\Sigma}^0$, Ξ^- . One can see that the mesons and (anti-)baryons multiplicities grow rapidly with increasing energy. The production of particles at high energies is practically identical with respect to particles-antiparticles and mainly originates from the hadronization process of the Quark-Gluon Plasma. With decreasing energy one can see a separation between baryons and antibaryons which comes from baryon stopping, from possible $B - \bar{B}$ annihilations, and from the fact that antibaryons (especially multi-strange baryons) are preferentially produced by the hadronization process from the QGP and, thus, more sensitive to the (T, μ_B) properties of the QGP partons.

5.1 | Directed and elliptic flows

As follows from hydrodynamical calculations (Bernhard, Moreland, Bass, Liu, & Heinz, 2016; Marty, Bratkovskaya, Cassing, Aichelin, & Berrehrh, 2013; Romatschke & Romatschke, 2007; H. Song & Heinz, 2008) and the Bayesian analysis (Bernhard et al., 2016), the results for the flow harmonics v_n are sensitive to the transport coefficients. Recently we investigated the sensitivity of the collective flow (v_1 , v_2) coefficients to the μ_B dependences of partonic cross sections of DQPM which provide the η/s and ζ/s consistent with IQCD results as discussed in Section 2. For that we calculated v_1 , v_2 for different identified hadrons - mesons and (anti-) baryons (Soloveva, Moreau, Oliva, Song, et al., 2020; Soloveva, Moreau, Oliva, Voronyuk, et al., 2020).

We start with presenting the results of our study (Soloveva, Moreau, Oliva, Song, et al., 2020; Soloveva, Moreau, Oliva,

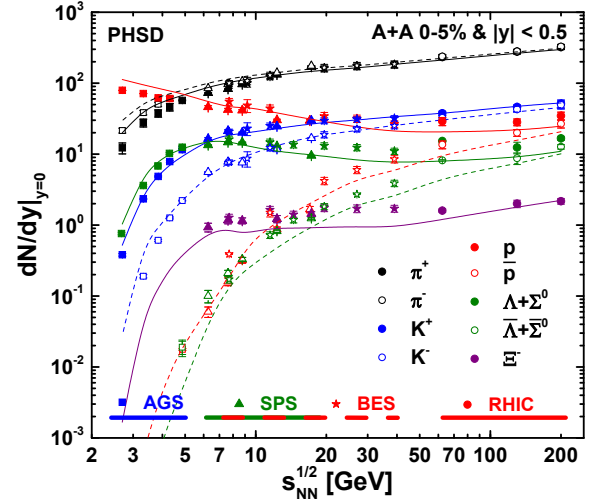


FIGURE 5 Excitation function $(dN/dy)|_{y=0}$ of particles produced in central heavy-ion collisions at midrapidity from the PHSD (Moreau, 2019) in comparison with experimental data from E895 (Klay et al., 2002, 2003), E866-E917 (Ahle et al., 2000a, 2000b; Back et al., 2001), E896 (Albergo et al., 2002) and E895 (Pinkenburg et al., 2002) collaborations at AGS energies, from the NA49 (Afanasiev et al., 2002; Alt et al., 2005, 2006, 2008a, 2008b) and the NA57 (Antinori et al., 2004) collaborations for SPS energies, and from the STAR collaboration for the Beam-Energy-Scan (Adamczyk et al., 2017; Ashraf, 2016) and top RHIC regimes (Abelev et al., 2009; Adcox et al., 2002; Aggarwal et al., 2011).

Voronyuk, et al., 2020) for the traces of μ_B dependences of the QGP interaction cross sections in the directed flow. Fig. 6 depicts the directed flow v_1 of identified hadrons (K^\pm , p , \bar{p} , $\Lambda + \Sigma^0$, $\bar{\Lambda} + \bar{\Sigma}^0$) versus rapidity for Au+Au collisions at $\sqrt{s_{NN}} = 27$ GeV. One can see a good agreement between PHSD results and experimental data from the STAR collaboration (Adamczyk et al., 2018). However, the different versions of PHSD for the v_1 coefficients show a quite similar behavior; only antihyperons indicate a slightly different flow. This supports again the finding that strangeness, and in particular anti-strange hyperons, are the most sensitive probes for the QGP properties.

We continue with presenting the results for the elliptic flow of charged hadrons from heavy-ion collisions within the PHSD5.0. In Fig. 7 we display the elliptic flow v_2 of identified hadrons (K^\pm , p , \bar{p} , $\Lambda + \Sigma^0$, $\bar{\Lambda} + \bar{\Sigma}^0$) as a function of p_T at $\sqrt{s_{NN}} = 27$ GeV for PHSD4.0 (green lines), PHSD5.0 with partonic cross sections and parton masses calculated for $\mu_B = 0$ (blue dashed lines) and with cross sections and parton masses evaluated at the actual chemical potential μ_B in each individual space-time cell (red lines) in comparison to the experimental data of the STAR Collaboration (Adamczyk et al., 2016). Similar to the directed flow shown in Fig. 6, the elliptic flow

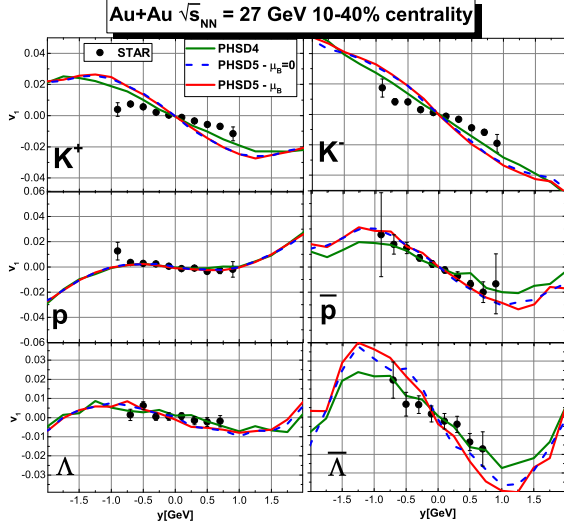


FIGURE 6 Directed flow of identified hadrons as a function of rapidity for Au+Au collisions at $\sqrt{s_{NN}} = 27$ GeV for PHSD4.0 (green lines), PHSD5.0 with partonic cross sections and parton masses calculated for $\mu_B = 0$ (blue dashed lines) and with cross sections and parton masses evaluated at the actual chemical potential μ_B in each individual space-time cell (red lines) in comparison to the experimental data of the STAR Collaboration (Adamczyk et al., 2018).

from all three scenarios in the PHSD shows a rather similar behavior; the differences are very small (within the statistics achieved here). Only antiprotons and antihyperons show a tendency for a small decrease of the v_2 at larger p_T for PHSD5.0 compared to PHSD4.0, which can be attributed to the explicit \sqrt{s} -dependence and different angular distribution of partonic cross sections in the PHSD5.0. We note that the underestimation of v_2 for protons and Λ 's might be attributed to details of the hadronic vector potentials involved in this calculations which seem to underestimate the baryon repulsion. We also attribute the slight overestimation of antibaryon v_2 to the lack of baryon potential.

In this study we also explore the lower collision energy $\sqrt{s_{NN}} = 14.5$ GeV and present in Fig. 8 the results for the v_2 of identified hadrons ($\pi^\pm, K^\pm, p, \bar{p}, \Lambda + \Sigma^0, \bar{\Lambda} + \bar{\Sigma}^0$) as a function of p_T . We find the same tendency as in Fig. 7 and show explicitly the PHSD4.0 (orange dashed lines) and the PHSD5.0 calculations with cross sections and parton masses depending on μ_B (blue solid lines) in comparison to the experimental data of the STAR Collaboration (Adam et al., 2020).

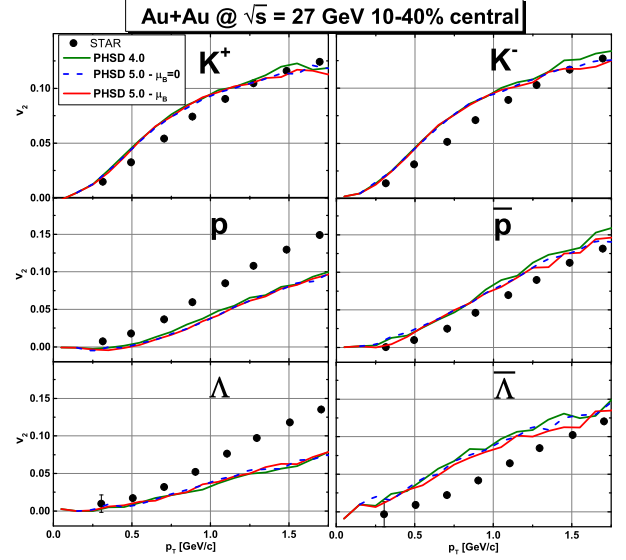


FIGURE 7 Elliptic flow of identified hadrons ($K^\pm, p, \bar{p}, \Lambda + \Sigma^0, \bar{\Lambda} + \bar{\Sigma}^0$) as a function of p_T for Au+Au collisions at $\sqrt{s_{NN}} = 27$ GeV for PHSD4.0 (green lines), PHSD5.0 with partonic cross sections and parton masses calculated for $\mu_B = 0$ (blue dashed lines) and with cross sections and parton masses evaluated at the actual chemical potential μ_B in each individual space-time cell (red lines) in comparison to the experimental data of the STAR Collaboration (Adamczyk et al., 2016).

6 | CONCLUSIONS

In this study we have reviewed the thermodynamic properties of the QGP as created in heavy-ion collisions and reported on the influence of the baryon chemical potential μ_B on the experimental observables such as the directed and elliptic flow.

For the description of the QGP we have employed the extended Dynamical QuasiParticle Model (DQPM) that is matched to reproduce the IQCD equation-of-state versus temperature T at zero and finite baryon chemical potential μ_B . We recall that the ratios η/s and ζ/s from the DQPM agree very well with the IQCD results from Ref. (Astrakhantsev et al., 2018) and show a similar behavior as the ratio obtained from a Bayesian fit (Bernhard et al., 2016). As found previously in Refs. (Moreau et al., 2019; Soloveva, Moreau, & Bratkovskaya, 2020) the transport coefficients show only a mild dependence on μ_B .

Our study of the heavy-ion collisions, i.e. non-equilibrium QGP, has been performed within the extended Parton-Hadron-String Dynamics (PHSD) transport approach (Moreau et al., 2019) in which the properties of quarks and gluons, i.e. their masses and widths, depend on T and μ_B explicitly. Moreover, the partonic interaction cross sections

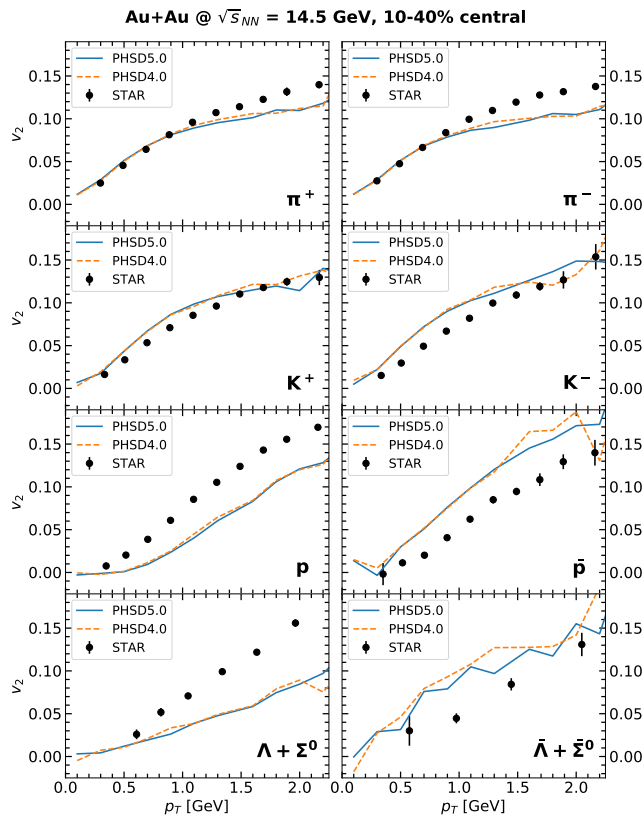


FIGURE 8 Elliptic flow of identified hadrons (π^\pm , K^\pm , p , \bar{p} , $\Lambda + \Sigma^0$, $\bar{\Lambda} + \bar{\Sigma}^0$) as a function of p_T for Au+Au collisions at $\sqrt{s_{NN}} = 14.5$ GeV for the PHSD4.0 (orange dashed lines) and the PHSD5.0 with cross sections and parton masses depending on μ_B (blue solid lines) in comparison to the experimental data of the STAR Collaboration (Adam et al., 2020).

are obtained by evaluation of the leading order Feynman diagrams from the DQPM effective propagators and couplings and explicitly depend on the invariant energy \sqrt{s} as well as T and μ_B .

We have demonstrated the time evolution of heavy-ion collisions and $T - \mu_B$ trajectories as obtained from the PHSD5.0 calculations for SPS energies. We have explored the energy dependence of the averaged μ_B around the chemical freeze-out temperature and found a reasonable agreement with statistical model results (Adamczyk et al., 2017; Andronic et al., 2010; Cleymans et al., 2006).

We have explored the sensitivity of heavy-ion observables such as the excitation function of the hadron multiplicities and collective flow coefficients v_1 , v_2 on the (T, μ_B) dependence of the QGP properties. After remarking that the sensitivity (w.r.t. the μ_B -dependence) of hadronic rapidity and p_T distributions of hadrons for symmetric and asymmetric heavy-ion collisions from AGS to RHIC energies was found to be very low (Moreau

et al., 2019; Soloveva, Moreau, & Bratkovskaya, 2020), we have discussed the sensitivity of the collective flow of hadrons. As an example, we have shown the results for $\sqrt{s_{NN}} = 14.5$ and 27 GeV. As has been shown in Refs. (Soloveva, Moreau, Oliva, Song, et al., 2020; Soloveva, Moreau, Oliva, Voronyuk, et al., 2020) we find only very small differences between the results from PHSD4.0 and from PHSD5.0 on the hadronic flow observables at high as well as at intermediate energies. This is related to the fact that at high energies, where the matter is dominated by the QGP, one probes only a small baryon chemical potential in central collisions at midrapidity, while at lower energies (and larger μ_B) the fraction of the QGP drops rapidly (cf. Fig. 3) such that in total the final observables are dominated by the hadronic interactions and thus the information about the partonic properties and scatterings is washed out. This finding is also consistent with the fact that the transport coefficients - as evaluated in the DQPM - show only a weak dependence on μ_B . We have shown that the mild μ_B -dependence of QGP interactions is more pronounced in observables for strange hadrons (kaons and especially anti-strange hyperons) which provides an experimental hint for the search of μ_B traces of the QGP for experiments at the future FAIR/NICA facilities and the BESII program at RHIC.

ACKNOWLEDGEMENTS

The authors acknowledge inspiring discussions with Jörg Aichelin, Wolfgang Cassing, Ilya Selyuzhenkov and Arkadiy Taranenko. The computational resources have been provided by the LOEWE-Center for Scientific Computing and the "Green Cube" at GSI, Darmstadt. P.M. acknowledges support by the U.S. D.O.E. under Grant No. DE-FG02-05ER41367. O.S., I.G. acknowledge support from HGS-HIRE for FAIR. L.O. has been financially supported by the Alexander von Humboldt Foundation. Furthermore, we acknowledge support by the Deutsche Forschungsgemeinschaft (DFG, German Research Foundation): grant BR 4000/7-1, grant CRC-TR 211 'Strong-interaction matter under extreme conditions' - Project number 315477589 - TRR 211; by the Russian Science Foundation grant 19-42-04101; by the European Union's Horizon 2020 research and innovation program under grant agreement No 824093 (STRONG-2020) and by the COST Action THOR, CA15213.

REFERENCES

- Aarts, G., & Martinez Resco, J. M. 2002, *JHEP*, 04, 053. doi:
- Abelev, B., et al. 2009, *Phys. Rev. C*, 79, 034909. doi:
- Adam, J., et al. 2020, *Phys. Rev. C*, 101(2), 024905. doi:
- Adamczyk, L., et al. 2016, *Phys. Rev. C*, 93(1), 014907. doi:
- Adamczyk, L., et al. 2017, *Phys. Rev. C*, 96(4), 044904. doi:

- Adamczyk, L., et al. 2018, *Phys. Rev. Lett.*, 120(6), 062301. doi:
- Adcox, K., et al. 2002, *Phys. Rev. Lett.*, 89, 092302. doi:
- Afanasiev, S. V., et al. 2002, *Phys. Rev. C*, 66, 054902. doi:
- Aggarwal, M., et al. 2011, *Phys. Rev. C*, 83, 024901. doi:
- Ahle, L., et al. 2000a, *Phys. Lett.*, B490, 53-60. doi:
- Ahle, L., et al. 2000b, *Phys. Lett.*, B476, 1-8. doi:
- Albergo, S., et al. 2002, *Phys. Rev. Lett.*, 88, 062301. doi:
- Albright, M., & Kapusta, J. 2016, *Phys. Rev. C*, 93(1), 014903. doi:
- Alt, C., et al. 2005, *Phys. Rev. Lett.*, 94, 192301. doi:
- Alt, C., et al. 2006, *Phys. Rev.*, C73, 044910. doi:
- Alt, C., et al. 2008a, *Phys. Rev.*, C78, 034918. doi:
- Alt, C., et al. 2008b, *Phys. Rev.*, C77, 024903. doi:
- Andronic, A., Braun-Munzinger, P., & Stachel, J. 2010, *Nucl. Phys. A*, 834, 237C–240C. doi:
- Antinori, F., et al. 2004, *Phys. Lett.*, B595, 68-74. doi:
- Aoki, Y., Borsanyi, S., Durr, S., Fodor, Z., Katz, S. D., Krieg, S., & Szabo, K. K. 2009, *JHEP*, 06, 088. doi:
- Aoki, Y., Endrodi, G., Fodor, Z., Katz, S., & Szabo, K. 2006, *Nature*, 443, 675–678. doi:
- Ashraf, M. U. 2016, *J. Phys. Conf. Ser.*, 668(1), 012095. doi:
- Astrakhantsev, N., Braguta, V., & Kotov, A. 2017, *JHEP*, 04, 101. doi:
- Astrakhantsev, N., Braguta, V., & Kotov, A. 2018, *Phys. Rev. D*, 98(5), 054515. doi:
- Back, B., et al. 2001, *Phys. Rev. Lett.*, 87, 242301. doi:
- Bazavov, A., et al. 2012, *Phys. Rev. D*, 85, 054503. doi:
- Bernard, C., Burch, T., Gregory, E. et al. 2005, *Phys. Rev. D*, 71, 034504. doi:
- Bernhard, J. E., Moreland, J. S., Bass, S. A., Liu, J., & Heinz, U. 2016, *Phys. Rev. C*, 94(2), 024907. doi:
- Berrehrah, H., Bratkovskaya, E., Steinert, T., & Cassing, W. 2016, *Int. J. Mod. Phys. E*, 25(07), 1642003. doi:
- Borsanyi, S., Endrodi, G., Fodor, Z., Katz, S., Krieg, S., Ratti, C., & Szabo, K. 2012, *JHEP*, 08, 053. doi:
- Borsanyi, S., Fodor, Z., Hoelbling, C., Katz, S. D., Krieg, S., & Szabo, K. K. 2014, *Phys. Lett. B*, 730, 99–104. doi:
- Bratkovskaya, E., Cassing, W., Konchakovski, V., & Linnyk, O. 2011, *Nucl. Phys. A*, 856, 162–182. doi:
- Bratkovskaya, E., Kostyuk, A., Cassing, W., & Stoecker, H. 2004, *Phys. Rev. C*, 69, 054903. doi:
- Cassing, W. 2007a, *Nucl. Phys. A*, 795, 70–97. doi:
- Cassing, W. 2007b, *Nucl. Phys. A*, 791, 365–381. doi:
- Cassing, W. 2009, *Eur. Phys. J. ST*, 168, 3–87. doi:
- Cassing, W., & Bratkovskaya, E. 1999, *Phys. Rept.*, 308, 65–233. doi:
- Cassing, W., & Bratkovskaya, E. 2008, *Phys. Rev. C*, 78, 034919. doi:
- Cassing, W., & Bratkovskaya, E. 2009, *Nucl. Phys. A*, 831, 215–242. doi:
- Cassing, W., Palmese, A., Moreau, P., & Bratkovskaya, E. 2016, *Phys. Rev. C*, 93, 014902. doi:
- Chakraborty, P., & Kapusta, J. 2011, *Phys. Rev. C*, 83, 014906. doi:
- Cleymans, J., Oeschler, H., Redlich, K., & Wheaton, S. 2006, *Phys. Rev. C*, 73, 034905. doi:
- Fernandez-Fraile, D., & Gomez Nicola, A. 2006, *Phys. Rev. D*, 73, 045025. doi:
- Fuseau, D., Steinert, T., & Aichelin, J. 2020, *Phys. Rev. C*, 101(6), 065203. doi:
- Gavin, S. 1985, *Nucl. Phys. A*, 435, 826–843. doi:
- Guenther, J., Bellwied, R., Borsanyi, S. et al. 2017, *Nucl. Phys. A*, 967, 720–723. doi:
- Guenther, J. N. 2020, 10,
- Hosoya, A., & Kajantie, K. 1985, *Nucl. Phys. B*, 250, 666–688. doi:
- Kadanoff, L., & Baym, G. 1962, *Benjamin, New York*, 203 pp.
- Klahn, T., et al. 2006, *Phys. Rev. C*, 74, 035802. doi:
- Klay, J. L., et al. 2002, *Phys. Rev. Lett.*, 88, 102301. doi:
- Klay, J. L., et al. 2003, *Phys. Rev.*, C68, 054905. doi:
- Kubo, R. 1957, *J. Phys. Soc. Jap.*, 12, 570–586. doi:
- Kumar, L. 2011, *J. Phys. G*, 38, 124145. doi:
- Lang, R., Kaiser, N., & Weise, W. 2015, *Eur. Phys. J. A*, 51(10), 127. doi:
- Linnyk, O., Bratkovskaya, E., & Cassing, W. 2016, *Prog. Part. Nucl. Phys.*, 87, 50–115. doi:
- Linnyk, O., Konchakovski, V., Cassing, W., & Bratkovskaya, E. 2013, *Phys. Rev. C*, 88, 034904. doi:
- Marty, R., Bratkovskaya, E., Cassing, W., Aichelin, J., & Berrehrah, H. 2013, *Phys. Rev. C*, 88, 045204. doi:
- Mohanty, B. 2011, *J. Phys. G*, 38, 124023. doi:
- Moreau, P. 2019. Dynamical description of relativistic heavy-ion collisions out-of-equilibrium (Unpublished doctoral dissertation). Goethe U., Frankfurt (main).
- Moreau, P., Soloveva, O., Oliva, L., Song, T., Cassing, W., & Bratkovskaya, E. 2019, *Phys. Rev. C*, 100(1), 014911. doi:
- Ozvenchuk, V., Linnyk, O., Gorenstein, M., Bratkovskaya, E., & Cassing, W. 2013, *Phys. Rev. C*, 87(2), 024901. doi:
- Palmese, A., Cassing, W., Seifert, E., Steinert, T., Moreau, P., & Bratkovskaya, E. 2016, *Phys. Rev. C*, 94(4), 044912. doi:
- Peshier, A., & Cassing, W. 2005, *Phys. Rev. Lett.*, 94, 172301. doi:
- Pinkenburg, C., et al. 2002, *Nucl. Phys.*, A698, 495-498. doi:
- Romatschke, P., & Romatschke, U. 2007, *Phys. Rev. Lett.*, 99, 172301. doi:
- Soloveva, O., Moreau, P., & Bratkovskaya, E. 2020, *Phys. Rev. C*, 101(4), 045203. doi:
- Soloveva, O., Moreau, P., Oliva, L., Song, T., Cassing, W., & Bratkovskaya, E. 2020, *J. Phys. Conf. Ser.*, 1602(1), 012012. doi:
- Soloveva, O., Moreau, P., Oliva, L., Song, T., Cassing, W., & Bratkovskaya, E. 2019, 11, Transport coefficients of hot and dense matter. 18th International Conference on Strangeness in Quark Matter.
- Soloveva, O., Moreau, P., Oliva, L., Voronyuk, V., Kireyeu, V., Song, T., & Bratkovskaya, E. 2020, *Particles*, 3(1), 178–192. doi:
- Song, H., & Heinz, U. W. 2008, *Phys. Rev. C*, 78, 024902. doi:
- Song, T., Cassing, W., Moreau, P., & Bratkovskaya, E. 2018, *Phys. Rev. C*, 97(6), 064907. doi:
- Strassmeier, K., Brandenburg, A., Cuntz, M., Hasinger, G., Montmerle, T., & Neuhäuser, R. (Eds.). 2019, Proceedings, 8th International Workshop on Astronomy and Relativistic Astrophysics (IWARA2018): Ollantaytambo, Peru, September 8-15, 2018 (Vol. 340) (No. 1-3).
- Vanderheyden, B., & Baym, G. 1998, *J. Statist. Phys.*, 93, 843. doi:

How cite this article: P. Moreau et al. (2021), Properties of the QGP created in heavy-ion collisions, *Astronomische Nachrichten*, 2021;.

How cite this article: P. Moreau et al. (2021), Properties of the QGP created in heavy-ion collisions, *Astronomische Nachrichten*, 2021;.